PNAS RESEARCH ARTICLE | CELL BIOLOGY OPEN ACCESS

CCAR2 functions downstream of the Shieldin complex to promote double-strand break end-joining

Divya Ramalingam Iyer[a], Naoya Harada[a], Connor Clairmont[a], Lige Jiang[a], David Martignetti[a,b], Huy Nguyen[a,b], Yizhou Joseph He[a], Dipanjan Chowdhury[a], and Alan D. D'Andrea[a,b,c,1]

Contributed by Alan D. D'Andrea; received August 31, 2022; accepted October 31, 2022; reviewed by Daniel Durocher and Andre Nussenzweig

The 53BP1-RIF1 pathway restricts the resection of DNA double-strand breaks (DSBs) and promotes blunt end-ligation by non-homologous end joining (NHEJ) repair. The Shieldin complex is a downstream effector of the 53BP1-RIF1 pathway. Here, we identify a component of this pathway, CCAR2/DBC1, which is also required for restriction of DNA end-resection. CCAR2 co-immunoprecipitates with the Shieldin complex, and knockout of CCAR2 in a BRCA1-deficient cell line results in elevated DSB end-resection, RAD51 loading, and PARP inhibitor (PARPi) resistance. Knockout of CCAR2 is epistatic with knockout of other Shieldin proteins. The S1-like RNA-binding domain of CCAR2 is required for its interaction with the Shieldin complex and for suppression of DSB end-resection. CCAR2 functions downstream of the Shieldin complex, and CCAR2 knockout cells have delayed resolution of Shieldin complex foci. Forkhead-associated (FHA)-dependent targeting of CCAR2 to DSB sites re-sensitized BRCA1−/−SHLD2−/− cells to PARPi. Taken together, CCAR2 is a functional component of the 53BP1-RIF1 pathway, promotes the refill of resected DSBs, and suppresses homologous recombination.

53BP1 | Shieldin complex | CCAR2/DBC1 | homologous recombination | single nucleotide variants

One of the most detrimental type of DNA damage in cells is double-strand breaks (DSBs). If left unrepaired, DSBs can lead to loss of genetic information and trigger genome instability (1–4). DSBs are primarily repaired by two major antagonistic DNA repair pathways—non-homologous end-joining (NHEJ) and homologous recombination (HR). NHEJ involves direct ligation of broken DNA ends and is generally error-prone as it creates indels, whereas HR is an error-free mechanism of DNA repair involving the use of the undamaged sister chromatid to repair the broken DNA ends (2, 3). The choice of DSB repair pathway has clinical implications and is determined by the tug-of-war between 53BP1-RIF1-Shieldin axis which promotes NHEJ and BRCA1 which favors HR (5).

BRCA1/2-deficient cancers are defective for HR repair and highly sensitive to poly(ADP-ribose) polymerase inhibitors (PARPi). Several PARPi have recently received FDA approval for breast and ovarian cancer treatment (6, 7). Despite the initial success, most BRCA1/2-deficient patients develop resistance against PARPi-based therapies. Thus, understanding the mechanisms by which cells develop resistance against PARPi is important for identifying ways to target breast and ovarian cancers.

One major mechanism by which BRCA1-deficient tumors gain resistance against PARPi is via down-regulation of factors involved in NHEJ (8, 9). Loss of any of the factors that promote NHEJ—53BP1, REV7, SHLD1, SHLD2, or SHLD3—in a BRCA1-deficient background makes cells resistant to PARPi. BRCA1 promotes DNA end-resection, a critical step needed to initiate HR, while 53BP1 counters it and promotes DNA end-protection (10, 11). Several groups have shown that 53BP1 recruits the Shieldin complex to protect the DNA ends from extensive resection mediated by DNA2/EXO1 (12–21). Furthermore, Shieldin recruits CST-Polα to fill-in the resected ends and to generate structures compatible for end-joining (17, 22). More recently, Zhao et al. have shown that SHLD2 can also recruit ASTE1, an endonuclease, to trim the length of the resected DNA ends and to improve filling by CST-Polα, an enzyme with limited processivity (23, 24).

SHLD2 has three OB-folds which allow it to bind to the resected single-stranded DNA ends and prevent further resection (12, 16, 18, 19). CST-Polα-mediated filling-in converts the resected single-stranded DNA to double-stranded DNA and presumably dislodges SHLD2 from the DNA. The precise mechanism of the Shieldin pathway and how CST-Polα-mediated refill prevents further DSB end-resection is unknown.

A key multifaceted player in this pathway is REV7, which is a subunit of the Shieldin complex and of the Polζ complex, a translesion polymerase functioning in the Fanconi pathway (25, 26). Recently, the protein Cell cycle and apoptosis regulator 2 (CCAR2)/deleted in breast cancer 1 (DBC1) was identified by IP-mass spectrometry as an additional interactor of REV7 (18, 27).

Significance

PARP inhibition induces synthetic lethality in homologous recombination (HR)-deficient cells. PARP inhibitors (PARPi) have received regulatory approval for treatment of BRCA1/2-deficient tumors. However, emergence of acquired and de novo resistance against PARPi is a major hurdle in the clinic. The Shieldin complex was recently discovered as a critical player in mediating PARPi sensitivity in BRCA1−/− cells. Here, we report a new player, CCAR2 as an effector in the Shieldin pathway. Loss of CCAR2 in BRCA1−/− cells leads to robust resistance against PARPi and mitomycin C treatment. CCAR2 is a suppressor of HR and single nucleotide variants (SNVs). Finally, CCAR2 is frequently deleted in patients and its loss correlates with poor prognosis, thus underscoring the importance of our study.

Competing interest statement: The authors declare no competing interest. A.D.D. reports consulting for Acerand Therapeutics, AstraZeneca, Bayer AG, Blacksmith/Lightstone Ventures, Bristol Myers Squibb, Cedilla Therapeutics, Constellation Pharmaceuticals, Cyteir Therapeutics, EMD Serono, Epizyme, Faze Medicines, GlaxoSmithKline, Impact Therapeutics, LAV Global Management Company Limited, PrimeFour Therapeutics, Patheon Pharmaceuticals, Pfizer, Tango Therapeutics, and Zentalis Pharmaceuticals/Zeno Management; is an Advisory Board member for Cedilla Therapeutics, Cyteir, and Impact Therapeutics; stockholder in Cedilla Therapeutics, Cyteir, Impact Therapeutics, and PrimeFour Therapeutics; and reports receiving commercial research grants from Bristol Myers Squibb, EMD Serono, Moderna, and Tango Therapeutics.

[1]To whom correspondence may be addressed. Email: alan_dandrea@dfci.harvard.edu.

This article contains supporting information online at https://www.pnas.org/lookup/suppl/doi:10.1073/pnas.2214935119/-/DCSupplemental.

Published November 29, 2022.

CCAR2 was originally identified as DBC1. CCAR2 is localized to a region on human chromosome 8p21 that is frequently deleted in breast cancer (28). This finding led to the assumption that the gene functions as a tumor suppressor. However, the role of CCAR2 in tumor progression is controversial. Overexpression or reduced expression of CCAR2, both are associated with poor prognosis across various tumor types (29–32). Although the exact role of CCAR2 in tumorigenesis has been elusive, the gene is highly altered in several different cancer types (*SI Appendix*, Fig. S5*A*). Thus, understanding the mechanism by which CCAR2 promotes or suppresses tumor formation is critical.

CCAR2 affects diverse biological processes such as transcription, RNA splicing, circadian rhythm, metabolism, apoptosis, and B-cell development (30–34). The well-studied role of CCAR2 related to tumorigenesis is in apoptosis. In response to DNA damage, CCAR2 is phosphorylated at Thr454 by the ataxia telangiectasia mutated (ATM) or ATM- and Rad3-related (ATR) kinase. Phosphorylated CCAR2 inhibits deacetylase SIRT1 and thereby promotes p53 acetylation, which triggers p53-dependent apoptosis (35, 36). Interestingly, a genome-wide screen identified CCAR2 as a factor that favors NHEJ over HR (37). However, contradictory to this finding, another study demonstrated that CCAR2 promotes HR (38). Thus, the role of CCAR2 in DNA repair remains largely unresolved.

In the current study, we identify CCAR2 as an interactor of the REV7-Shieldin complex and demonstrate that it functions downstream of the Shieldin pathway to promote end-joining. CCAR2 loss phenocopies Shieldin loss by promoting end-resection and PARPi resistance in BRCA1-deficient cells. The S1-like domain of CCAR2 mediates the interaction with the REV7-Shieldin complex. Loss of NHEJ promoting factors, such as 53BP1, Shieldin, or CCAR2, also makes BRCA1-deficient cells resistant to mitomycin C (MMC) and cisplatin treatment. Finally, CCAR2 loss in a BRCA1-deficient tumor correlates with increased single nucleotide variants (SNVs) and poor prognosis for the corresponding cancer patient.

Results

CCAR2 Interacts with the Shieldin Complex. We previously purified tandem-affinity-tagged REV7 complexes and analyzed them using mass spectrometry (27). Interestingly, one of the top hits was the CCAR2/DBC1/KIAA1967 protein (30, 33). CCAR2 was also identified in another recent mass spectrometry screen for REV7-binding proteins (18). Since REV7 is known to bind to the SHLD1, SHLD2, and SHLD3 proteins to form the Shieldin complex, we reasoned that CCAR2 might function directly or indirectly with this complex. The Shieldin complex is localized to sites of DNA DSBs where it inhibits DSB end-resection, blocks HR, and promotes NHEJ (12–21). Disruption of the Shieldin complex, either by knockout of REV7, SHLD1, SHLD2, or SHLD3, or by overexpression of TRIP13 ATPase or of CHAMP1, results in enhanced DSB end-resection and HR repair (27, 39–41).

We initially tested whether CCAR2 is also a component of the Shieldin complex (Fig. 1). As predicted from the mass spectrometry results (18, 27), pulldown of FLAG-tagged REV7 resulted in co-immunoprecipitation of the endogenous CCAR2 and the TRIP13 ATPase from 293T cell lysates (Fig. 1*A*). We also confirmed the interaction of CCAR2 and REV7 by reciprocal immunoprecipitation with FLAG-tagged CCAR2 (*SI Appendix*, Fig. S1*A*). In our previous work, we had demonstrated that REV7 exists in two conformation (open and closed) and that the closed conformation binds to the seat–belt interactors SHLD3, REV3, and CHAMP1 (27, 41). The AAA+ATPase TRIP13 catalyzes the conversion of closed-REV7 to open-REV7 (27). Accordingly, we tested whether TRIP13 affects the interaction of CCAR2 with REV7. TRIP13 overexpression or TRIP13 knockdown did not affect the interaction of CCAR2 with REV7, suggesting that CCAR2 is not a seat–belt interactor (*SI Appendix*, Fig. S1 *B* and *C*). Interestingly, GFP-tagged SHLD3, SHLD2, or SHLD1 also immunoprecipitated CCAR2 (Fig. 1 *B*–*D*), further suggesting the possible relevance of CCAR2 to functions of the Shieldin complex. CCAR2 co-immunoprecipitated more strongly with SHLD1 and SHLD2 protein than with the SHLD3 protein. Overall, CCAR2 co-immunoprecipitated with the Shieldin complex, suggesting its functional relevance in the 53BP1-RIF1 pathway.

CCAR2 is an Inhibitor of HR. Disruption of the Shieldin complex results in an increase in DSB end-resection and enhancement in HR repair in BRCA1-deficient cells, resulting in PARPi resistance (12–21). To test the possible role of CCAR2 in the regulation of HR repair, we initially generated BRCA1 knockout cells and confirmed their sensitivity to PARPi and to cross-linking agents MMC and cisplatin (Fig. 1 *E* and *F* and *SI Appendix*, Fig. S1 *D* and *G*). Interestingly, knockout of CCAR2 restored PARPi and MMC resistance in these cells (Fig. 1 *E* and *F*). Furthermore, the enhancement of PARPi resistance or MMC (or cisplatin) resistance resulting from CCAR2 knockout was similar to the increase observed by knockout of SHLD2 or SHLD3 (Fig. 1 *E* and *F* and *SI Appendix*, Fig. S1 *G*–*J*). Knockdown of CCAR2 also resulted in an increase in PARPi resistance in BRCA1-deficient high-grade serous ovarian carcinoma cancer cell lines, UWB1.289 and COV362 (*SI Appendix*, Fig. S1 *E* and *F*). Double CRISPR knockout of CCAR2 and SHLD3 in BRCA1-deficient cells resulted in the same level of PARPi resistance or MMC (or cisplatin) resistance as the level from SHLD3 knockout alone, further demonstrating that CCAR2 and SHLD3 function in an epistatic manner (Fig. 1 *E* and *F* and *SI Appendix*, Fig. S1*G*). Taken together, loss of CCAR2 promotes drug resistance in BRCA1-deficient cells, similar to the effect of Shieldin complex loss.

CCAR2 Knockout Increases HR Repair. To more directly determine the activity of CCAR2 in HR repair, we next used the DR-GFP template assay (Fig. 2 *A*–*C*) (42). Knockdown of CCAR2 in U2OS cells expressing the DR-GFP cassette caused an increase in HR capacity, consistent with a previous report (Fig. 2*A* and *SI Appendix*, Fig. S2*A*) (37). CCAR2 depletion also restored HR capacity in BRCA1-depleted cells, similar to the effect of 53BP1 or SHLD2 depletion (Fig. 2*B*) (11, 18, 20). We further corroborated this observation in RPE cells transfected with the DR-GFP vector (*SI Appendix*, Fig. S2*B*). Loss of CCAR2 increased HR capacity in BRCA1-deficient cells (*SI Appendix*, Fig. S2*B*). Knockdown of CCAR2 did not restore HR activity of BRCA2-depleted cells (Fig. 2*C*), further demonstrating that CCAR2 is a negative regulator of DSB end-resection, a prerequisite for HR activity.

To test the role of CCAR2 directly on end-resection, we performed the AsiSI assay with U2OS DIvA cells (43). Knockdown of CCAR2 using three different siRNA consistently increased end-resection, as compared to scrambled siRNA (Fig. 2*D* and *SI Appendix*, Fig. S2*D*). This result is again consistent with a previous study showing increased RPA accumulation at AsiSI-induced breaks in CCAR2-depleted U2OS DIvA cells (Fig. 2*D* and *SI Appendix*, Fig. S2*D*) (37).

The increase in HR activity resulting from CCAR2 knockout correlated with an increase in the level of the MRE11/RAD50/

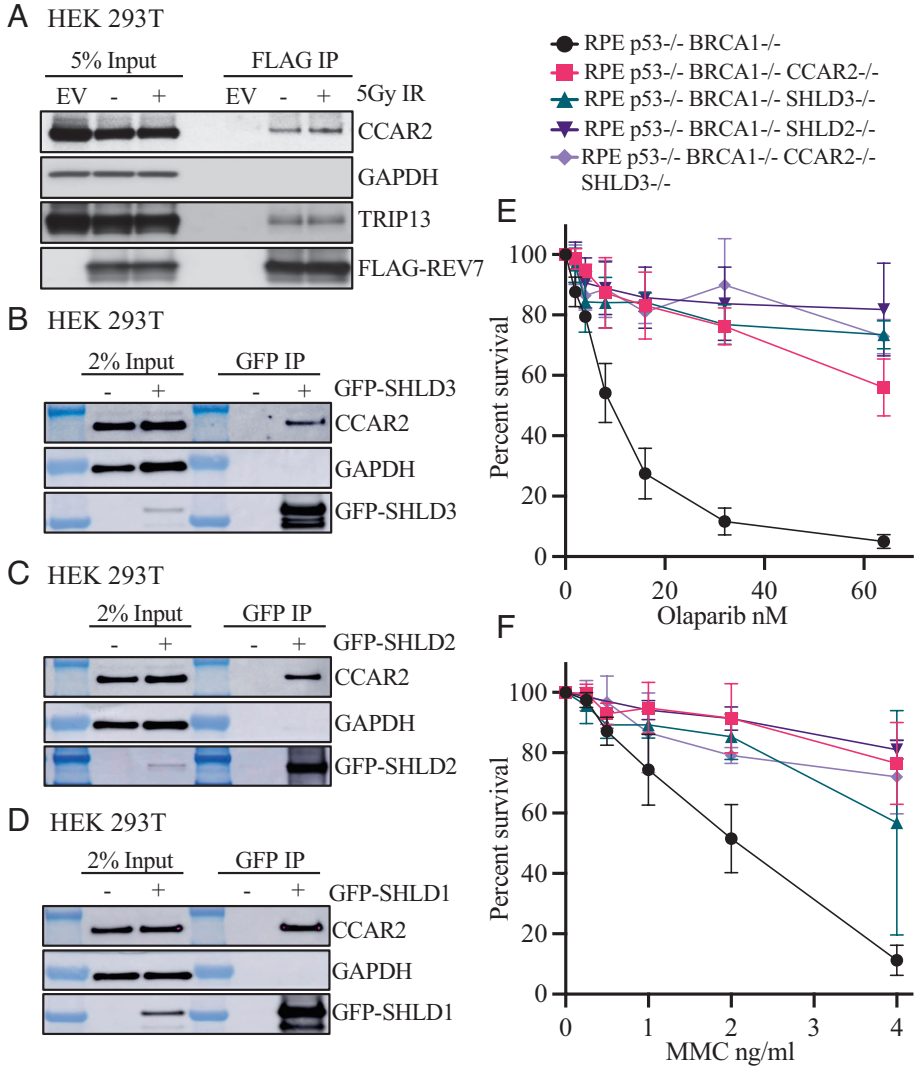

Fig. 1. CCAR2 Interacts with Shieldin and its Loss Confers PARPi and MMC resistance in BRCA1−/− cells. (*A*) CCAR2 interacts with REV7. HEK 293T cells were transfected with FLAG-REV7. 48 h after transfection, cells were irradiated with 5 Gy and samples were harvested 1 h post-IR and FLAG IP was performed. Representative images showing co-immunoprecipitation of CCAR2 with REV7. Three biologically independent experiments were performed. (*B–D*) CCAR2 interacts with SHLD3, SHLD2, and SHLD1. HEK 293T cells transfected with GFP-SHLD3 (*B*), GFP-SHLD2 (*C*), or GFP-SHLD1 (*D*), respectively. Samples were processed for GFP-IP. Representative images showing co-immunoprecipitation of CCAR2 with GFP-SHLD3 (*B*), GFP-SHLD2 (*C*), or GFP-SHLD1 (*D*), respectively. Three biologically independent experiments were performed. (*E–F*) CCAR2 loss promotes resistance against PARPi and MMC treatment. Cell survival assays were performed with the various CRISPR knockout clones to test sensitivity toward Olaparib (*E*) and MMC (*F*). Error bars represent standard deviations between multiple replicates performed with multiple independent knockout clones as listed below. RPE p53−/−BRCA1−/− (n = 7); RPE p53−/−BRCA1−/−CCAR2−/− 3 independent clones (n = 5); RPE p53−/−BRCA1−/−SHLD3−/− 3 independent clones (n = 2); RPE p53−/−BRCA1−/−SHLD2−/− 2 independent clones (n = 2); RPE p53−/−BRCA1−/−CCAR2−/−SHLD3−/− 3 independent clones—2 polyclonal and 1 clonal (n = 2).

NBS1 complex on the chromatin (Fig. 2*E*), a nuclease complex required for the early events in HR repair. Consistent with this result, a previous study indicated that CCAR2 is a negative regulator of the CTIP-MRN complex and may block DSB end-resection through this activity (37). CCAR2 knockout also resulted in an enhanced accumulation of PARPi-induced and IR-induced RAD51 foci (Fig. 2*F* and *SI Appendix*, Fig. S2 *C* and *E–H*). Taken together, CCAR2 knockout, like Shieldin knockout, increased DSB end-resection and promoted HR repair.

The CCAR2 S1 Domain is Required for Shieldin Complex Binding and for Re-Sensitization of CCAR2−/− Cells to PARPi and MMC. CCAR2 is a highly conserved nuclear protein in eukaryotes. It is composed of several domains, namely, a S1-like putative RNA-binding domain, a nuclear localization signal (NLS), a leucine zipper (LZ) domain, an inactive Nudix hydrolase domain, an inactive EF hand, and a coiled coil segment (Fig. 3*A*). The presence of multiple domains may allow CCAR2 to perform its diverse biological processes such as apoptosis, DNA repair, transcription, metabolism, circadian cycle, and B cell development (30–34).

In an attempt to identify DNA repair functions associated with a specific domain of CCAR2, we initially generated a series of deletion mutants (Fig. 3 *A* and *B*). These mutants were co-expressed in HEK 293T cells along with the GFP-tagged REV7 protein. GFP immunoprecipitation analysis demonstrated that the S1-like putative RNA-binding domain of CCAR2 is required for interaction with REV7 (Fig. 3*B*). Unlike the wildtype CCAR2 protein, the S1 deletion mutant (m2) failed to co-immunoprecipitate with GFP-SHLD3, GFP-SHLD2, or GFP-SHLD1 (*SI Appendix*, Fig. S3 *A–C*), indicating that the S1 domain is

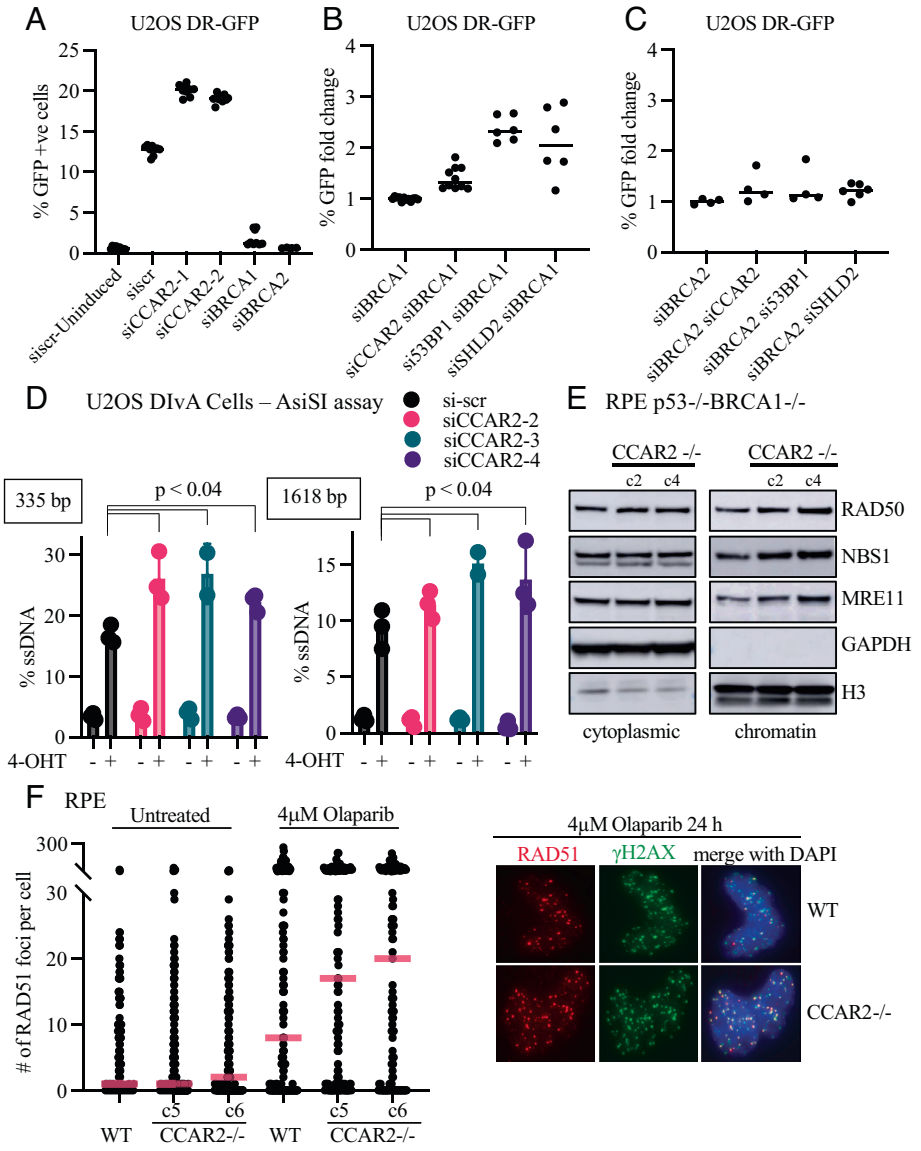

Fig. 2. CCAR2 Loss Promotes HR. (*A*) Loss of CCAR2 promotes HR. Assessment of gene conversion by DR-GFP assay. Effect of CCAR2 knockdown was evaluated using two different siRNAs. BRCA1 and BRCA2 knockdown were used as controls. Data points represent individual values obtained from three independent experiments with three technical replicates in each experiment. (*B–C*) Loss of CCAR2 promotes HR in BRCA1 knockdown. Assessment of gene conversion by DR-GFP assay. Rescue of HR capacity in BRCA1 knockdown (*B*) and BRCA2 knockdown (*C*) was assessed by co-depleting either CCAR2, 53BP1, or SHLD2. Multiple siRNA (2–3) were used for CCAR2, 53BP1, and SHLD2. The percentage of GFP-positive cells in each condition was normalized to that from BRCA1 knockdown (*B*) or BRCA2 knockdown (*C*) condition. Two independent experiments were performed. Individual values from an experiment are plotted. (*D*) Loss of CCAR2 promotes DNA end-resection. DNA end-resection was quantified in U2OS DIvA cells depleted of CCAR2 using three different siRNA. DNA end-resection around DSB1 was measured using qPCR as described in *Materials and Methods*. Three independent experiments were performed with three technical replicates in each. Error bars represent standard deviation between replicates. Statistical analysis was performed using two-tailed unpaired Student's *t* test. (*E*) Loss of CCAR2 increases MRN on the chromatin. RPE p53−/−BRCA1−/− and two independent clones of RPE p53−/−BRCA1−/−CCAR2−/− were subjected to cellular fractionation. The cytoplasmic and chromatin fractions were run on 4–12% SDS-PAGE gel and probed for the indicated proteins. (*F*) Loss of CCAR2 promotes PARPi-induced RAD51 focus formation. RPE wild-type and two independent RPE CCAR2−/− clones were treated with 4 μM Olaparib for 24 h. After treatment, cells were fixed and stained for γH2AX (green) and RAD51 (red). Number of foci per nuclei were counted using custom scripts on Cell Profiler. More than 100 cells were quantified for each condition. Two biologically independent experiments were performed. Quantification is represented on the *Left* panel, and the *Right* panel shows representative images.

required, either directly or indirectly, for the interaction of CCAR2 with the Shieldin complex.

The wildtype CCAR2 and S1 deletion mutant of CCAR2 (m2) were also tested for their ability to restore PARPi sensitivity or MMC sensitivity in RPE p53−/−BRCA1−/−CCAR2−/− knockout cells. Interestingly, the S1 domain of CCAR2 was also critical for restoring drug sensitivity (Fig. 3 *C* and *D* and *SI Appendix*, Fig. S3*D*). Taken together, the interaction of CCAR2 with the Shieldin complex is required for the restriction of DSB end-resection and for the inhibition of HR repair.

DNA Damage-Inducible Assembly of the Shieldin Complex in the Absence of CCAR2. We reasoned that CCAR2, like the recently-identified endonuclease ASTE1, might be recruited to DSBs where it prevents DSB end-resection and favors re-blunting of DSBs (Fig. 4*C*). To test this model, we initially asked whether the Shieldin complex can assemble in the absence of CCAR2 (Fig. 4*A* and *SI Appendix*, Fig. S4 *A–C*). We evaluated the interaction of SHLD3, SHLD2, SHLD1 with REV7 by immunoprecipitation and the recruitment of SHLD3 to damage sites in CCAR2 knockouts. Interestingly, loss of CCAR2 did not affect the interaction between REV7 and SHLD3, SHLD2,

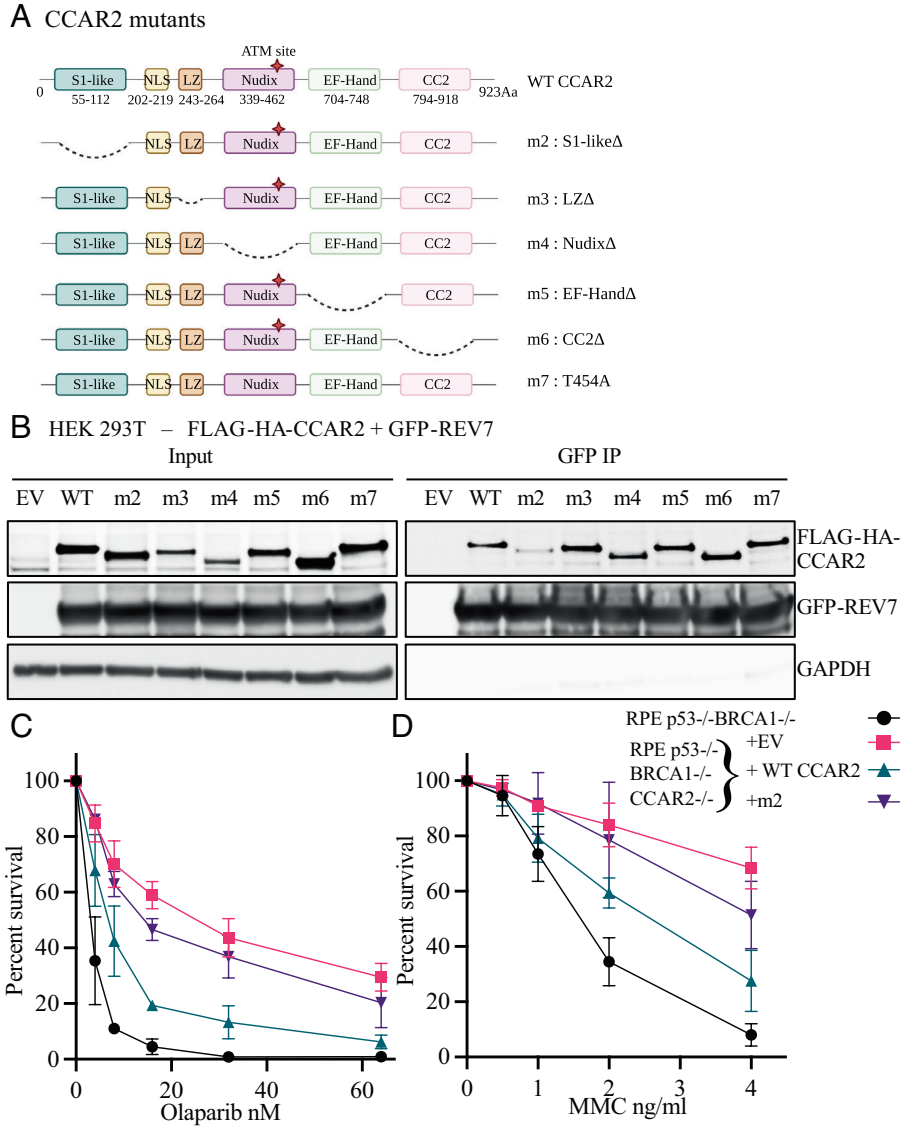

Fig. 3. CCAR2 is an Effector of Shieldin via its S1 Domain. (*A*) Schematic depiction of all the CCAR2 mutants generated and used in this study. (*B*) S1-domain of CCAR2 is important for interaction with REV7. HEK 293T cells were co-transfected with GFP-REV7 and full-length FLAG-HA-CCAR2 or various mutants of CCAR2. 48 h after transfection, cells were harvested and processed for GFP immunoprecipitation. Two biologically independent experiments were performed. Representative images showing co-immunoprecipitation of CCAR2 with REV7. (*C* and *D*) CCAR2 functions via S1-domain. RPE p53−/−BRCA1−/−CCAR2−/− cells complemented using retrovirus carrying empty vector, full-length CCAR2 or m2 mutant of CCAR2 were seeded for cell survival assays to test sensitivity toward Olaparib (*C*) or MMC (*D*). RPE p53−/−BRCA1−/− cells were included as control in the assay. Three biologically independent experiments were performed. Error bars represent standard deviation between replicates.

SHLD1 (*SI Appendix*, Fig. S4 *A*–*C*). DNA damage is known to promote the recruitment of SHLD3 to DSBs in a 53BP1- and RIF1-dependent manner (15, 18, 23). DNA damage from IR-induced similar levels of SHLD3 foci in RPE WT and CCAR2−/− cells (Fig. 4*A*). In summary, CCAR2 is not required for the assembly of the Shieldin complex or its recruitment to sites of damage.

We hypothesized that CCAR2 might therefore function downstream of the Shieldin complex to prevent end-resection (Fig. 4*C*). To test this idea, we evaluated the resolution of SHLD3 foci at various time points after IR (Fig. 4*A*). SHLD3 foci persisted in CCAR2−/− cells at later time points (4 h and 8 h) suggesting that completion of repair downstream of the Shieldin complex is suboptimal in these cells. These results further support a model in which CCAR2 functions downstream of the Shieldin complex (Fig. 4*C*). The SHLD3 foci persists after IR in these cells, apparently due to the persistence of unrepaired DSBs, as shown by the persistence of γH2AX foci (*SI Appendix*, Fig. S4*D*). The persistence of IR-inducible SHLD3 foci in CCAR2−/− cells is reminiscent of a similar observation in ASTE1−/− (23). In this regard, the loss of CCAR2 expression and the loss of ASTE1 expression have a similar phenotype.

The STN1-FHA and CCAR2-FHA Fusion Proteins Restore PARPi Sensitivity of the RPE-BRCA1(−/−) SHLD2(−/−) cells. We reasoned that if CCAR2 functions downstream of 53BP1 and the Shieldin complex, then targeting CCAR2 to DSB sites should rescue the phenotypes associated with Shieldin loss. To test this hypothesis, we used a method previously described for targeting proteins to DSBs by fusing the forkhead-associated (FHA) domain of RNF8 to CCAR2 (18, 22). In this way, the functional CCAR2 protein could be recruited to damaged chromatin independently of 53BP1 and the Shieldin complex.

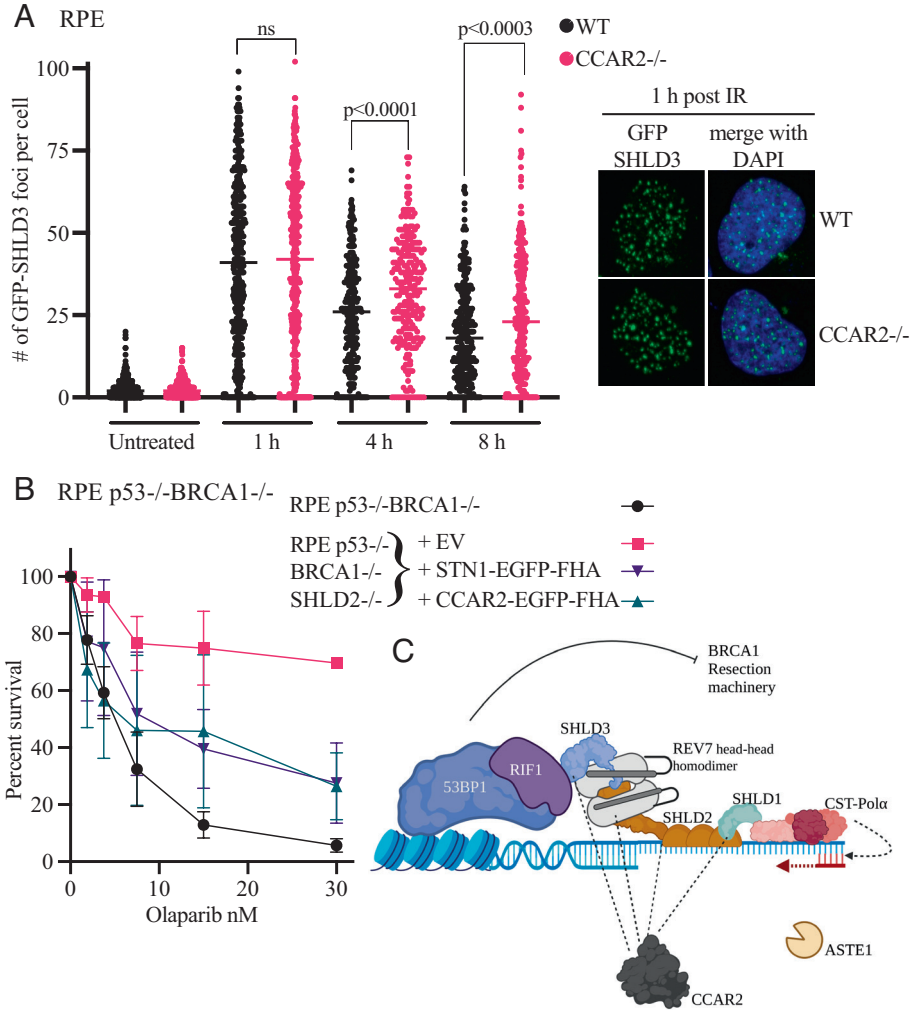

Fig. 4. CCAR2 is a Downstream Effector of the Shieldin Complex. (*A*) CCAR2 loss delays IR-induced SHLD3 foci resolution. RPE wild-type and CCAR2−/− cells were transduced with lentivirus carrying GFP-SHLD3. 48 h after transduction, cells were irradiated with 5Gy IR and harvested at various time points (1 h, 4 h, and 8 h) post-IR. Cells were fixed and stained for GFP and γH2AX. Number of foci per nuclei were counted using custom scripts on Cell Profiler. More than 100 cells were quantified for each condition. Two biologically independent experiments were performed. Statistical analysis was performed using two-tailed unpaired Student's *t* test. Quantification is represented on the *Left* panel, and the *Right* panel shows representative images. (*B*) CCAR2 functions downstream of the Shieldin complex. RPE p53−/−BRCA1−/−SHLD2−/− c2 clone was complemented using retrovirus carrying empty vector, CCAR2-EGFP-FHA or STN1-EGFP-FHA fusion construct. Cells were seeded for cell survival assay, and sensitivity toward Olaparib was tested. Three biologically independent experiments were performed. Error bars represent standard deviation between replicates. (*C*) Schematic illustration depicting CCAR2 acting downstream in the 53BP1-Shieldin pathway.

STN1 is known to function downstream of the Shieldin complex (17, 22). Therefore, we included STN1-FHA as a control in the assay. We found that the FHA-dependent targeting of CCAR2 to DSB sites partially re-sensitized the RPE p53−/−BRCA1−/−SHLD2−/− cells to PARPi (Fig. 4*B* and *SI Appendix*, Fig. S4*E*). The re-sensitization observed with CCAR2-FHA was similar to that observed by STN1-FHA. Taken together, these results suggest that CCAR2 mediates Shieldin complex-dependent DNA repair (Fig. 4*C*).

CCAR2 Loss in BRCA1-Deficient Tumors Correlates with Increased Signature 3 and Total SNV. The loss of CCAR2 promotes resistance of BRCA1-deficient cells to PARPi and to DNA cross-linking agents. To explore the clinical relevance of CCAR2 expression, we analyzed the landscape of genomic alterations in human tumors using The Cancer Genome Atlas (TCGA) datasets. Across various tumor types, CCAR2 is often deleted suggesting that its loss might confer growth advantage to cancer cells (*SI Appendix*, Fig. S5*A*).

Next, we evaluated BRCA1-deficient tumors to determine how loss of CCAR2 impacts the HR deficiency mutational signature (COSMIC single-base substitution Signature 3) and patient survival rates. BRCA1/2 loss is strongly associated with Signature 3 which serves as an HR deficiency (HRD) biomarker and has implications for patient treatment options. However, not all tumors with high Signature 3 have alterations in known HR factors, suggesting that unknown players may contribute toward the phenotype (44–48).

We selected ovarian cancer patients based on the expression levels of BRCA1/2 and CCAR2 in their tumors. As expected, BRCA1/2 "low" samples had higher levels of Signature 3 than BRCA1/2 "high" samples ($P = 0.00024$; Fig. 5*A*). Surprisingly, low CCAR2 levels in the BRCA1/2-deficient setting further increased Signature 3 levels ($P = 0.048$; Fig. 5*A*). Conversely, loss of BRCA1/2 expression in patients with low CCAR2 levels also increased Signature 3 levels ($P = 0.0041$; Fig. 5*A*). Thus, BRCA1/2 and CCAR2 expression loss have an additive effect on Signature 3 accumulation. Interestingly, we did not see a similar increase in mutational burden with 53BP1 expression loss in BRCA-deficient setting (*SI Appendix*, Fig. S5*B*). We observed a similar trend in total SNVs. Tumors with low CCAR2 levels in BRCA1/2-deficient setting carry a significantly high mutation burden ($P = 0.035$; Fig. 5*B*).

This result is counterintuitive since loss of CCAR2 increases HR and should therefore reduce Signature 3 levels in BRCA1/2

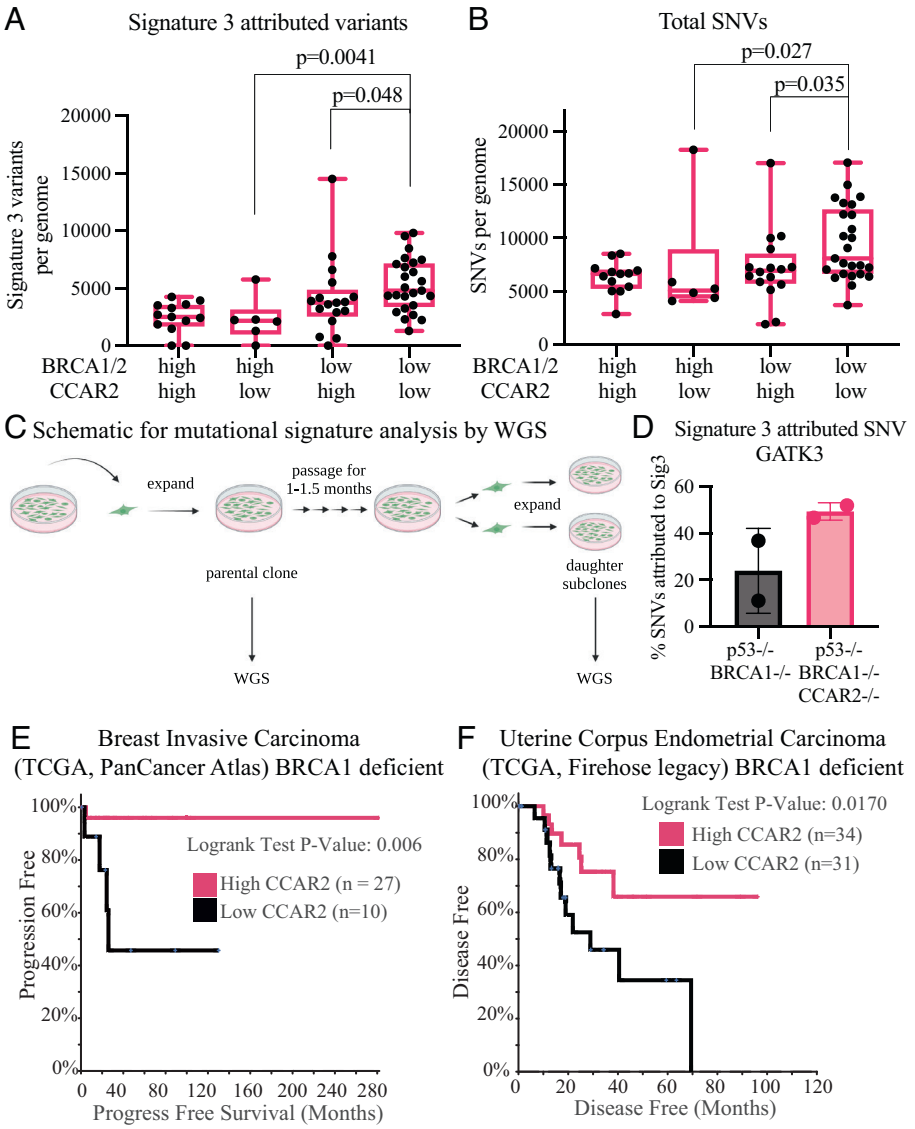

Fig. 5. CCAR2 loss Promotes Signature 3/SNVs in BRCA-Deficient Cancers and Correlates with Poor Patient Survival. (*A*) CCAR2 loss correlates with increased Signature 3 in patient samples. Ovarian cancer patient samples were sorted based on BRCA1/2 and CCAR2 expression levels as explained in the *Methods* section. Statistical analysis was performed using the Mann–Whitney test. (*B*) CCAR2 loss correlates with increased total SNV in patient samples. Ovarian cancer patient samples were sorted based on BRCA1/2 and CCAR2 expression levels as explained in the *Methods* section. Statistical analysis was performed using the Mann–Whitney test. (*C*) Schematic showing experimental setup for mutational signature analysis by whole genome sequencing. (*D*) CCAR2 loss increases Signature 3 attributed SNVs in BRCA1−/− cells. Total number of Signature 3 attributed SNVs were estimated from whole genome sequences of RPE p53−/− BRCA1−/− and RPE p53−/−BRCA1−/−CCAR2−/− cells using GATK3 algorithm. (*E* and *F*) Loss of CCAR2 in BRCA1-deficient patients correlates with poor progression- and disease-free survival rates. Breast invasive carcinoma (*E*) and uterine corpus endometrial carcinoma (*F*) patients deficient in BRCA1 were selected and further sorted based on CCAR2 expression levels (high and low) as described in the *Methods* section. Kaplan–Meier survival plots were generated comparing the patients with high and low CCAR2 levels using cBioPortal.

"low" patients. Although HR deficiency is tightly correlated with Signature 3, the exact etiology of Signature 3 mutational footprint is not understood (46, 49). Our finding suggests that CCAR2 may impact drug resistance by modulating other DNA repair pathways as well.

To further validate CCAR2's role in suppressing mutational burden, we performed whole genome sequencing (WGS) of RPE p53−/−BRCA1−/− and RPE p53−/−BRCA1−/−CCAR2−/− using a previously established strategy (45, 48, 50, 51) (Fig. 5 *C* and *D* and *SI Appendix*, Fig. S5 *C–E*). We isolated a single-cell clone (parental clone) and passaged it for ~ 6 wk followed by another round of single-cell isolation to derive the daughter subclones (Fig. 5*C*). By WGS of these clones, the loss of CCAR2 in BRCA1−/− cells increased Signature 3-attributed SNVs, consistent with the findings in the patient samples (Fig. 5 *A–D* and *SI Appendix*, Fig. S5 *C–E*).

CCAR2 Loss in BRCA1-Deficient Patients Correlates with Poor Prognosis. CCAR2 loss makes BRCA1-deficient cells resistant to PARPi and DNA crosslinking agents. Therefore, we hypothesized that loss of CCAR2 would have a detrimental effect on patient survival rates. To test this hypothesis, we looked at the survival of BRCA1-deficient patients in two different datasets—breast invasive carcinoma and uterine corpus endometrial carcinoma—and sorted them based on CCAR2 expression levels as described in the *Methods* section. As expected, BRCA1-deficient patients with low CCAR2 levels showed lower survival rates than those with high CCAR2 levels in both the datasets (Fig. 5 *E* and *F*). Taken

together, CCAR2 loss correlates with increased mutational burden in BRCA1-deficient patients and poor survival rates.

Discussion

CCAR2 is a Downstream Effector of the Shieldin Pathway. In the current study, we demonstrate that CCAR2/DBC1 interacts with the Shieldin complex and is a regulator of DNA repair pathway choice at DNA DSBs. The Shieldin complex assembles at DSBs, blocks DSB end-resection, and thereby inhibits RAD51 loading and HR repair. Knockout of any of the proteins in this complex, including REV7, SHLD1, SHLD2, SHLD3, or CCAR2, restores DSB end-resection and restores PARPi resistance in BRCA1-deficient cells (12–21). CCAR2 has an epistatic relationship with the proteins of the Shieldin complex (Fig. 1 *E* and *F* and *SI Appendix*, Fig. S1*G*). A double knockout of CCAR2 and SHLD3 results in a level of resistance against PARPi and DNA cross-link-inducing agents comparable to the single knockout of either gene.

Although CCAR2 co-immunoprecipitates with the Shieldin complex, the complex can assemble in the absence of CCAR2 (Fig. 1 *A*–*D* and *SI Appendix*, Fig. S4 *A*–*C*). Instead, our work demonstrates that CCAR2 is a downstream effector of the Shieldin complex. Targeting CCAR2 to DSB sites using the FHA domain of RNF8 can restore the 53BP1/Shieldin pathway and re-sensitize Shieldin-deficient cells to PARPi (Fig. 4*B*).

A recent study identified the DNA endonuclease, ASTE1, as another downstream effector of the Shieldin pathway (23). ASTE1 interacts directly with SHLD2 which is bound to ssDNA via OB folds. ASTE1 trims the 3′ overhang of the resected DNA DSB and presumably releases the Shieldin complex and completes the final steps in CST-mediated re-blunting of DSBs, required for the NHEJ pathway. The exact downstream role of CCAR2 in this pathway is less clear.

RNA Recruitment to Sites of DSB repair. The role of the S1 domain of CCAR2 in the 53BP1/Shieldin/CST pathway is unknown. On the one hand, the S1 domain is required for the co-immunoprecipitation of CCAR2 with the Shieldin complex (Fig. 3 *A* and *B* and *SI Appendix*, Fig. S3 *A*–*C*). On the other hand, the S1 domain, which is presumed to be an RNA-binding domain, may play a specific role in the pathway (30, 33). For instance, the S1 domain may play a role in recruiting an RNA molecule to the site of the DSB or interact with an RNA molecule at the vicinity of the break to impact repair dynamics.

Over the last 10 y, the importance of various RNA classes in the repair of DSBs has become increasingly evident (52–57). For instance, long non-coding RNAs (lncRNA) and microRNAs (miRNA) contribute to the repair of DSB, and DSB ends have been shown to produce damage-induced lncRNA (dilncRNA). RNA molecules at the site of a break vary in length and sequence and can adopt complex secondary structures. These structures can recruit diverse RNA-binding proteins and can promote phase separation, thereby providing a scaffold for the assembly of repair machinery. The role of RNA in DSB repair is still emerging and not fully understood. RNA molecules are hypothesized either to act as an anchor for the two DNA ends to enable end-joining or to recruit downstream effectors by enabling phase separation (52–57).

Several factors involved in the NHEJ pathway (KU heterodimer, 53BP1, RIF1, and DNA-PKcs) are either direct or indirect interactors of RNA and RNAPII (52–57). Interaction of KU with lncRNAs (LRIK and LINP1) promotes its recruitment to DNA breaks and also enhances recruitment of downstream effectors such as XRCC4 (58–60). Formation of damage-induced 53BP1 foci is also RNA-dependent (61, 62).

CCAR2, similar to other NHEJ factors, has intricate connections with RNA. It is a large disordered protein and a direct interactor of RNAPII (33, 63). A recent study showed that CCAR2 forms phase-separated nuclear bodies in an RNA transcript-dependent manner (64). Finally, lncRNA MALAT1 directly interacts with CCAR2 to modulate its effect on p53 via SIRT1 (65). It is plausible that CCAR2 via its interaction with dilncRNA may act as a bridge between the Shieldin pathway and the downstream NHEJ factors to promote DNA end-joining.

Role of CCAR2 in Drug Resistance. The common loss of CCAR2/DBC1 in breast and ovarian cancer (*SI Appendix*, Fig. S5*A*) suggests that the protein has a tumor suppressor function in these cancers. Consistent with this notion, the loss of CCAR2 in BRCA1-deficient tumors results in a worse prognosis (Fig. 5 *E* and *F*), further supporting the tumor suppressor model (66). It is important to note that our model of CCAR2's role in drug resistance is independent of its effect on p53 as most of our functional studies were carried out in RPE p53−/− BRCA1−/− background. Our data show that loss of CCAR2 can result in increased HR (Fig. 2 *A*–*F*) and in increased mutational burden (Fig. 5 *A*–*D*), thereby providing a mechanism for the tumor suppression by CCAR2. Our finding provides important implication for treatment of BRCA1-deficient patients.

CCAR2 may also have an impact on mutational burden indirectly, through its well-known role as a pro-apoptotic factor. Loss of CCAR2 in a tumor cell may decrease DNA damage-mediated apoptosis, leading to an overall increase in survival of cells with otherwise detrimental mutations. Thus, the elevated mutational burden of BRCA1-deficient cells with CCAR2 deficiency may result from a combination of an increased error-prone DNA repair mechanism, such as TLS (or increased SSA), plus an anti-apoptotic tendency.

In summary, CCAR2 is a multifunctional protein involved in diverse biological processes. Further studies are needed to elucidate the exact role of CCAR2 in the Shieldin pathway, via its putative RNA-binding domain. Emerging role of RNA in DNA repair coupled with recent development of RNA-based therapeutic interventions offers promise in tackling drug resistance mechanisms in the clinic.

Materials and Methods

Cell Culture. HEK293T, U2OS DR-GFP, COV362, U2OS DIvA, and Phoenix cells were grown in DMEM (Gibco) supplemented with 10% fetal bovine serum (FBS) (Sigma), 1% glutamine (Gibco), and 1% penicillin–streptomycin (Gibco). U2OS DR-GFP cells were a kind gift from Dr. Jeremy Stark, and U2OS DIvA cells were a kind gift from Dr. Gaëlle Legube.

RPE was grown in DMEM/F12-containing GlutaMAX (Gibco) and supplemented with 10% FBS and 1% penicillin–streptomycin. UWB1.289 was grown in a mixture of 50% RPMI 1640, 50% MEBM (Lonza) supplemented with MEGM singlequots supplements (Lonza) containing bovine pituitary extract, human epidermal growth factor, insulin, hydrocortisone, gentamicin sulfate-amphotericin, 3% FBS, and 1% penicillin–streptomycin. All cells were cultured in an incubator maintained at 37°C, 5% CO_2, and a relative humidity of 95%.

Plasmids. pDEST-FRT/TO-3xFLAG-REV7, pCW-eGFP-SHLD1, pCW-eGFP-SHLD2, and pCW-eGFP-SHLD3 were a kind gift from Dr. Daniel Durocher (Addgene # 114127, 114116, 114119, 114126). pDRGFP (Addgene # 26475) was a kind gift from Dr. Maria Jasin. psPAX2 and pMD2.G (Addgene # 12260, 12259) were a kind gift from Dr. Didier Trono.

Expression of SHLD1, SHLD2, and SHLD3 was induced by adding doxycycline–1 ug/ml. pCMV6-TRIP13-Myc-DDK was purchased from Origene

(RC201285). CCAR2 was cloned into pOZ-N using XhoI/NotI cloning sites. CCAR2 deletion mutants were generated by site-directed mutagenesis. G-block of STN1 fused to EGFP-FHA was synthesized and cloned into pOZ vector.

Plasmid transfection into HEK 293T cells was performed using Lipofectamine LTX with Plus reagent (Thermo Fisher Scientific). For RPE cells, plasmids were transduced using lentiviral or retroviral particles. All the plasmids used and generated in this study are listed in *SI Appendix*, Table S1.

Virus Generation. For all virus generation and transductions, media supplemented with heat-inactivated FBS was used. Lentivirus was generated by co-transfecting lentiviral constructs (pCW) with packaging vectors–psPAX2 and pMD2.G into HEK 293T cells using Lipofectamine LTX with Plus reagent. Retrovirus was generated by co-transfecting retroviral constructs (pOZ) with packaging vectors–pCG-Gag-pol and pCG-VsVg into Phoenix cells using Lipofectamine LTX with Plus reagent. 48 h and 72 h after transfection, supernatant containing virus was harvested, filtered through 0.45 μm filter. Viral transductions were performed in the presence of 8 ug/ml polybrene (Sigma). Cells were assayed for expression of constructs 48–72 h after viral transduction by flow cytometry or immuno-blotting.

Whole Cell Lysate, Cell Fractionation, and Immuno-Blotting. Whole cell lysate was prepared by lysing cells in ice-cold RIPA buffer (Cell Signaling Technology) supplemented with protease and phosphatase inhibitors (Cell Signaling Technology). Samples were processed for immuno-blotting as described in the *SI Appendix*.

Cell fractionation was performed using subcellular protein fractionation kit for cultured cells (Thermo Fisher Scientific) as described in the *SI Appendix*.

Antibodies and Drugs. All the antibodies and drugs used in this study are listed in *SI Appendix*, Tables S2 and S3, respectively.

siRNA Transfections. All siRNA transfections were performed using Lipofectamine RNAiMAX (ThermoFisher Scientific). siRNA was transfected at a final concentration of 20 nM. For DR-GFP assay, only one round of siRNA transfection was performed. For colony formation assays and immunoprecipitations, two rounds of siRNA transfections were performed. All siRNAs used in this study are listed in *SI Appendix*, Table S4.

CRISPR. All sgRNAs were ordered from Invitrogen. Single or multiple sgRNA targeting a gene along with TrueCut Cas9 Protein v2 (Invitrogen) were transfected into cells of choice using Lipofectamine CRISPRMAX (Invitrogen) according to manufacturer's instructions. Media was changed the following day. 72 h after transfection, the knockout pool cells were sorted into 96-well plates for single clone isolation. Knockout pool cells were also harvested for genomic editing analysis using Synthego ICE analysis platform as well as via immuno-blotting. *SI Appendix*, Tables S5 and S6 list all the gRNAs and primers used for generation and verification of knockouts, respectively. All the SHLD3 and SHLD2 knockout cell lines generated in this study are clonal except RPE p53−/−BRCA1−/−CCAR2−/−SHLD3−/− clones c7 and c8–which are polyclonal (*SI Appendix*, Fig. S1*I*). However, in both cases all the SHLD3 alleles show frameshift mutation, and therefore, c7 and c8 are null for SHLD3 (*SI Appendix*, Fig. S1*I*).

Immunoprecipitation (IP). HEK 293T cells were transfected with 4–10 μg of plasmid using Lipofectamine LTX with Plus reagent. Media was changed the next day after transfection. 48 h after transfection, cells were harvested using trypsin, washed with PBS, and stored at −80°C. RPE cells were transduced with lentiviral or retroviral constructs for immunoprecipitation. Cells were harvested 48 h after transduction. IP was performed as described in the *SI Appendix*.

Colony Formation Assays. Cells were seeded in 6-well plates. The number of cells seeded per well for the various genotypes are listed in *SI Appendix*, Table S7. The day after seeding, media containing drug was added. Plates were incubated for 8 or 9 d. After incubation, plates were washed twice with PBS, fixed in a mixture of methanol: acetic acid (5 : 1) for 20 min. The fixed cells were stained with crystal violet (Sigma) for 6 h to overnight and then washed with water twice. The plates were imaged on GE Amersham Imager 600 using colorimetric transillumination setting. The area fraction of the colonies in each well was estimated using ImageJ.

Cassette Reporter Assays. DR-GFP assay was performed as described previously (42). U2OS DR-GFP cells were a kind gift from Dr. Jeremy Stark. 75,000 cells were seeded per well in a 6-well plate on day 1. For each condition, three wells were seeded as technical replicates. An extra-set of triplicate wells were seeded for si-scramble condition. This extra set will not be subjected to I-SceI induction and serves as the negative control for the assay. On day 2, cells were transfected with siRNA. On day 3, cells were infected with adenovirus expressing I-SceI. Media was changed 5–6 h after virus transduction. On day 5, cells were trypsinized, harvested, re-suspended in 2% FBS (in PBS), and filtered. Samples were acquired on CytoFlex machine. Forward scatter and side scatter were used to gate the live, single-cell population. The si-scramble control without I-SceI induction was used as control to gate GFP-positive population.

AsiSI Assay. U2OS DIvA cells were a kind gift from Dr. Gaëlle Legube. Young passage cells (<10) were used for performing the assays. Assay was largely performed as described previously (43). 100,000 cells were seeded in a 6-cm dish on day 1. Three dishes were seeded for each condition–two plates for with and without (Z)-4-hydroxytamoxifen (4-OHT) induction and one plate to check knockdown efficiency by immuno-blotting. siRNA transfections were performed on day 2 and 3. On day 4, ER-AsiSI was induced by adding ~ 333nM 4-OHT. Cells were incubated with 4-OHT for 4 h. Cells were harvested by trypsinization, washed with PBS, and stored at −80°C. Genomic DNA was extracted using DNeasy Blood and Tissue kit (Qiagen). Genomic DNA was treated with RNaseH and then incubated with and without BsrGI-HF (NEB) restriction enzyme overnight at 37°C. qPCR was set up with the restriction enzyme digested and undigested DNA samples using Power SYBR Green Master mix (Thermo Fisher Scientific). End-resection was measured at the DSB1 break site (Chr 1: 89231183) which gets cleaved with high efficiency. Primers flanking the BsrGI sites at 335 bp and 1,618 bp away from the DSB1 break was used to set up the qPCR (*SI Appendix*, Table S8). For each sample, ΔCt was obtained by subtracting the Ct value of the undigested DNA sample from the Ct value of the digested DNA sample. The percentage of resected DNA (ssDNA%) was calculated as ssDNA% = (1/(2^(ΔCt − 1) + 0.5)) * 100.

Immunofluorescence. Cells were seeded on glass coverslips (Fisherbrand) in six well plates. Cells were irradiated or treated with drugs 24–48 h after seeding. For GFP-SHLD3 foci experiments, RPE cells transduced with GFP-SHLD3 lentivirus were used and expression was induced by adding doxycycline 1 ug/ml. For GFP-SHLD3 foci, cells were harvested at various timepoints (1 h, 2 h, 4 h, and 8 h) after 5-Gy irradiation. For RAD51 foci, cells were harvested 4 h post-5-Gy irradiation and 24 h after 4 μM Olaparib treatment. The cells were stained for GFP-SHLD3, RAD51, and γH2AX as described in the *SI Appendix*.

Whole Genome Sequencing and SNV Analysis. Previously established strategy was used for generating samples for mutational signature analysis (Fig. 5*C*) (45, 50, 51). Briefly, single-cell clones were isolated from RPE p53−/−, RPE p53−/−BRCA1−/−, and RPE p53−/−BRCA1−/−CCAR2−/− cell lines. The single-cell clone was expanded, and samples were harvested for sequencing. This sample is referred to as the parental clone (Fig. 5*C*). The parental clone was expanded and passaged for ~ 6 wk. After growing for 6 wk, single-cell clones were isolated from the parental clone to derive the daughter subclones (Fig. 5*C*). From each parent, two daughter cell subclones were derived, expanded, and harvested for sequencing (Fig. 5*C*). Genomic DNA was prepared from the parental and daughter subclones using DNeasy Blood and Tissue kit (Qiagen). In the final step, DNA was eluted in UltraPure DNase/RNase-free H_2O instead of buffer AE so that the EDTA (in Buffer AE) doesn't interfere with the subsequent library preparation steps. Whole genome sequencing and data analysis were performed as described in the *SI Appendix*.

Signature 3 and SNV Analysis in Patient Data. The association analyses between mutation counts and mRNA expression in ovarian tumors were performed using the mutation counts and the RNASeq expression data obtained from the Ovarian Cancer-Australia (OV-AU) project of the International Cancer Genome Consortium (ICGC) Pan-Cancer Analysis of Whole Genomes (PCAWG) study (https://dcc.icgc.org/releases/PCAWG/; retrieved 2/2020) as described in the *SI Appendix*.

TCGA Data Analysis. Survival data analysis from the breast invasive carcinoma (TCGA, PanCancer Atlas) dataset and uterine corpus endometrial carcinoma (TCGA, Firehose legacy) dataset was done using the cBioPortal website as described in the *SI Appendix* (67, 68).

Software. All illustrations in this manuscript were created using BioRender. Prism was used for generating all graphs. ImageJ was used for quantifying cell survival assays. Cell Profiler was used for analyzing all immunofluorescence images. cBioPortal was used for TCGA patient data analysis.

Data, Materials, and Software Availability. Whole genome sequencing data generated in this study are deposited in the Synapse database under the accession code syn45097852

ACKNOWLEDGMENTS. We thank all members of the D'Andrea laboratory for their helpful suggestions and comments. This work was supported by grants from the US National Institutes of Health (R01HL052725), the Gray Foundation (002085-0001-14759), the Breast Cancer Research Foundation (BCRF-20-033), the Ludwig Center at Harvard, the Smith Family Foundation (to A.D.D.), and the TESARO Post-Doctoral Fellowship Award from the Foundation for Women's Cancer (to D.R.I).

Author affiliations: [a]Division of Radiation and Genome Stability, Department of Radiation Oncology, Dana-Farber Cancer Institute, Harvard Medical School, Boston, MA 02215; [b]Center for DNA Damage and Repair, Dana-Farber Cancer Institute, Harvard Medical School, Boston, MA 02215; and [c]Department of Medical Oncology, Dana-Farber Cancer Institute, Harvard Medical School, Boston, MA 02215

Author contributions: D.R.I., C.C., D.C., and A.D.D. designed research; D.R.I., N.H., L.J., D.M., and Y.J.H. performed research; D.R.I. contributed new reagents/analytic tools; D.R.I., N.H., H.N., and A.D.D. analyzed data; and D.R.I. and A.D.D. wrote the paper.

Reviewers: D.D., Mount Sinai Hospital; and A.N., National Cancer Institute.

1. A. Ciccia, S. J. Elledge, The DNA damage response: Making it safe to play with knives. *Mol. Cell* **40**, 179–204 (2010).
2. R. Scully, A. Panday, R. Elango, N. A. Willis, DNA double-strand break repair-pathway choice in somatic mammalian cells. *Nat. Rev. Mol. Cell Biol.* **20**, 698–714 (2019).
3. R. Ceccaldi, B. Rondinelli, A. D. D'Andrea, Repair pathway choices and consequences at the double-strand break. *Trends Cell Biol.* **26**, 52–64 (2016).
4. S. R. Kieffer, N. F. Lowndes, Immediate-early, early, and late responses to DNA double stranded breaks. *Front. Genet.* **13**, 793884 (2022).
5. D. Setiaputra, D. Durocher, Shieldin–The protector of DNA ends. *EMBO Rep.* **20**, e47560 (2019).
6. T. A. Yap, R. Plummer, N. S. Azad, T. Helleday, The DNA damaging revolution: PARP inhibitors and beyond. *Am. Soc. Clin. Oncol. Educ. Book* **39**, 185–195 (2019).
7. C. J. Lord, A. Ashworth, BRCAness revisited. *Nat. Rev. Cancer* **16**, 110–120 (2016).
8. M. P. Dias, S. C. Moser, S. Ganesan, J. Jonkers, Understanding and overcoming resistance to PARP inhibitors in cancer therapy. *Nat. Rev. Clin. Oncol.* **18**, 773–791 (2021).
9. K. Fugger, G. Hewitt, S. C. West, S. J. Boulton, Tackling PARP inhibitor resistance. *Trends Cancer* **7**, 1102–1118 (2021).
10. P. Bouwman *et al.*, 53BP1 loss rescues BRCA1 deficiency and is associated with triple-negative and BRCA-mutated breast cancers. *Nat. Struct. Mol. Biol.* **17**, 688–695 (2010).
11. S. F. Bunting *et al.*, 53BP1 inhibits homologous recombination in Brca1-deficient cells by blocking resection of DNA breaks. *Cell* **141**, 243–254 (2010).
12. S. Findlay *et al.*, SHLD2/FAM35A co-operates with REV7 to coordinate DNA double-strand break repair pathway choice. *EMBO J.* **37**, e100158 (2018).
13. S. Gao *et al.*, An OB-fold complex controls the repair pathways for DNA double-strand breaks. *Nat. Commun.* **9**, 3925 (2018).
14. H. Ghezraoui *et al.*, 53BP1 cooperation with the REV7-shieldin complex underpins DNA structure-specific NHEJ. *Nature* **560**, 122–127 (2018).
15. R. Gupta *et al.*, DNA repair network analysis reveals Shieldin as a key regulator of NHEJ and PARP inhibitor sensitivity. *Cell* **173**, 972–988.e923 (2018).
16. J. Tomida *et al.*, FAM35A associates with REV7 and modulates DNA damage responses of normal and BRCA1-defective cells. *EMBO J.* **37**, e99543 (2018).
17. Z. Mirman *et al.*, 53BP1-RIF1-shieldin counteracts DSB resection through CST- and Polalpha-dependent fill-in. *Nature* **560**, 112–116 (2018).
18. S. M. Noordermeer *et al.*, The Shieldin complex mediates 53BP1-dependent DNA repair. *Nature* **560**, 117–121 (2018).
19. H. Dev *et al.*, Shieldin complex promotes DNA end-joining and counters homologous recombination in BRCA1-null cells. *Nat. Cell Biol.* **20**, 954–965 (2018).
20. G. Xu *et al.*, REV7 counteracts DNA double-strand break resection and affects PARP inhibition. *Nature* **521**, 541–544 (2015).
21. V. Boersma *et al.*, MAD2L2 controls DNA repair at telomeres and DNA breaks by inhibiting 5′ end resection. *Nature* **521**, 537–540 (2015).
22. Z. Mirman, N. K. Sasi, A. King, J. R. Chapman, T. de Lange, 53BP1-shieldin-dependent DSB processing in BRCA1-deficient cells requires CST-polalpha-primase fill-in synthesis. *Nat. Cell Biol.* **24**, 51–61 (2022).
23. F. Zhao *et al.*, ASTE1 promotes shieldin-complex-mediated DNA repair by attenuating end resection. *Nat. Cell Biol.* **23**, 894–904 (2021).
24. Y. He, J., D. Chowdhury, ASTE1 cutting to block DNA end resection. *Nat. Cell Biol.* **23**, 818–819 (2021).
25. C. S. Clairmont, A. D. D'Andrea, REV7 directs DNA repair pathway choice. *Trends Cell Biol.* **31**, 965–978 (2021).
26. I. de Krijger, V. Boersma, J. J. L. Jacobs, REV7: Jack of many trades. *Trends Cell Biol.* **31**, 686–701 (2021).
27. C. S. Clairmont *et al.*, TRIP13 regulates DNA repair pathway choice through REV7 conformational change. *Nat. Cell Biol.* **22**, 87–96 (2020).
28. M. Hamaguchi *et al.*, DBC2, a candidate for a tumor suppressor gene involved in breast cancer. *Proc. Natl. Acad. Sci. U.S.A.* **99**, 13647–13652 (2002).
29. P. Joshi, O. L. Quach, S. S. B. Giguere, I. M. Cristea, A functional proteomics perspective of DBC1 as a regulator of transcription. *J. Proteomics Bioinform.* **Suppl. 2**, 002 (2013).
30. M. Magni, G. Buscemi, L. Zannini, Cell cycle and apoptosis regulator 2 at the interface between DNA damage response and cell physiology. *Mutat. Res. Rev. Mutat. Res.* **776**, 1–9 (2018).
31. E. N. Chini, C. C. Chini, V. Nin, C. Escande, Deleted in breast cancer-1 (DBC-1) in the interface between metabolism, aging and cancer. *Biosci. Rep.* **33**, e00058 (2013).
32. G. S. Johnson, P. Rajendran, R. H. Dashwood, CCAR1 and CCAR2 as gene chameleons with antagonistic duality: Preclinical, human translational, and mechanistic basis. *Cancer Sci.* **111**, 3416–3425 (2020).
33. J. Brunquell, J. Yuan, A. Erwin, S. D. Westerheide, B. Xue, DBC1/CCAR2 and CCAR1 are largely disordered proteins that have evolved from one common ancestor. *Biomed Res. Int.* **2014**, 418458 (2014).
34. Q. Fang, J. A. Bellanti, S. G. Zheng, Advances on the role of the deleted in breast cancer (DBC1) in cancer and autoimmune diseases. *J. Leukoc Biol.* **109**, 449–454 (2021).
35. J. E. Kim, J. Chen, Z. Lou, DBC1 is a negative regulator of SIRT1. *Nature* **451**, 583–586 (2008).
36. W. Zhao *et al.*, Negative regulation of the deacetylase SIRT1 by DBC1. *Nature* **451**, 587–590 (2008).
37. A. Lopez-Saavedra *et al.*, A genome-wide screening uncovers the role of CCAR2 as an antagonist of DNA end resection. *Nat. Commun.* **7**, 12364 (2016).
38. M. Tanikawa *et al.*, Role of multifunctional transcription factor TFII-I and putative tumour suppressor DBC1 in cell cycle and DNA double strand damage repair. *Br J. Cancer* **109**, 3042–3048 (2013).
39. I. de Krijger *et al.*, MAD2L2 dimerization and TRIP13 control shieldin activity in DNA repair. *Nat. Commun.* **12**, 5421 (2021).
40. H. Fujita *et al.*, CHAMP1-POGZ counteracts the inhibitory effect of 53BP1 on homologous recombination and affects PARP inhibitor resistance. *Oncogene* **41**, 2706–2718 (2022).
41. F. Li *et al.*, CHAMP1 binds to REV7/FANCV and promotes homologous recombination repair. *Cell Rep.* **40**, 111297 (2022).
42. A. J. Pierce, R. D. Johnson, L. H. Thompson, M. Jasin, XRCC3 promotes homology-directed repair of DNA damage in mammalian cells. *Genes Dev.* **13**, 2633–2638 (1999).
43. Y. Zhou, P. Caron, G. Legube, T. T. Paull, Quantitation of DNA double-strand break resection intermediates in human cells. *Nucleic. Acids. Res.* **42**, e19 (2014).
44. P. Polak *et al.*, A mutational signature reveals alterations underlying deficient homologous recombination repair in breast cancer. *Nat. Genet.* **49**, 1476–1486 (2017).
45. A. Poti *et al.*, Correlation of homologous recombination deficiency induced mutational signatures with sensitivity to PARP inhibitors and cytotoxic agents. *Genome Biol.* **20**, 240 (2019).
46. J. Setton, J. S. Reis-Filho, S. N. Powell, Homologous recombination deficiency: How genomic signatures are generated. *Curr. Opin. Genet. Dev.* **66**, 93–100 (2021).
47. L. B. Alexandrov *et al.*, The repertoire of mutational signatures in human cancer. *Nature* **578**, 94–101 (2020).
48. G. Koh, A. Degasperi, X. Zou, S. Momen, S. Nik-Zainal, Mutational signatures: Emerging concepts, caveats and clinical applications. *Nat. Rev. Cancer* **21**, 619–637 (2021).
49. X. Hu, Z. Xu, S. De, Characteristics of mutational signatures of unknown etiology. *NAR Cancer* **2**, zcaa026 (2020).
50. O. Pipek *et al.*, Fast and accurate mutation detection in whole genome sequences of multiple isogenic samples with IsoMut. *BMC Bioinf.* **18**, 73 (2017).
51. G. Koh, X. Zou, S. Nik-Zainal, Mutational signatures: Experimental design and analytical framework. *Genome Biol.* **21**, 37 (2020).
52. C. Fijen, E. Rothenberg, The evolving complexity of DNA damage foci: RNA, condensates and chromatin in DNA double-strand break repair. *DNA Repair (Amst.)* **105**, 103170 (2021).
53. B. Zhao, E. Rothenberg, D. A. Ramsden, M. R. Lieber, The molecular basis and disease relevance of non-homologous DNA end joining. *Nat. Rev. Mol. Cell Biol.* **21**, 765–781 (2020).
54. M. Dutertre, S. Vagner, DNA-damage response RNA-binding proteins (DDRBPs): Perspectives from a new class of proteins and their RNA targets. *J. Mol. Biol.* **429**, 3139–3145 (2017).
55. C. Audoynaud, S. Vagner, S. Lambert, Non-homologous end-joining at challenged replication forks: An RNA connection? *Trends Genet.* **37**, 973–985 (2021).
56. S. Jimeno, F. R. Balestra, P. Huertas, The emerging role of RNA modifications in DNA double-strand break repair. *Front. Mol. Biosci.* **8**, 664872 (2021).
57. D. Zong, P. Oberdoerffer, P. J. Batista, A. Nussenzweig, RNA: A double-edged sword in genome maintenance. *Nat. Rev. Genet.* **21**, 651–670 (2020).
58. D. Wang *et al.*, LRIK interacts with the Ku70-Ku80 heterodimer enhancing the efficiency of NHEJ repair. *Cell Death Differ.* **27**, 3337–3353 (2020).
59. Y. Zhang *et al.*, Long noncoding RNA LINP1 regulates repair of DNA double-strand breaks in triple-negative breast cancer. *Nat. Struct. Mol. Biol.* **23**, 522–530 (2016).
60. A. B. Dalby, K. J. Goodrich, J. S. Pfingsten, T. R. Cech, RNA recognition by the DNA end-binding Ku heterodimer. *RNA* **19**, 841–851 (2013).
61. F. Michelini *et al.*, Damage-induced lncRNAs control the DNA damage response through interaction with DDRNAs at individual double-strand breaks. *Nat. Cell Biol.* **19**, 1400–1411 (2017).
62. S. Francia *et al.*, Site-specific DICER and DROSHA RNA products control the DNA-damage response. *Nature* **488**, 231–235 (2012).
63. P. Close *et al.*, DBIRD complex integrates alternative mRNA splicing with RNA polymerase II transcript elongation. *Nature* **484**, 386–389 (2012).
64. T. Mannen *et al.*, Distinct RNA polymerase transcripts direct the assembly of phase-separated DBC1 nuclear bodies in different cell lines. *Mol. Biol. Cell* **32**, ar33 (2021).
65. R. Chen *et al.*, Quantitative proteomics reveals that long non-coding RNA MALAT1 interacts with DBC1 to regulate p53 acetylation. *Nucleic. Acids Res.* **45**, 9947–9959 (2017).
66. B. Qin *et al.*, DBC1 functions as a tumor suppressor by regulating p53 stability. *Cell Rep.* **10**, 1324–1334 (2015).
67. J. Gao *et al.*, Integrative analysis of complex cancer genomics and clinical profiles using the cBioPortal. *Sci. Signal.* **6**, pl1 (2013).
68. E. Cerami *et al.*, The cBio cancer genomics portal: An open platform for exploring multidimensional cancer genomics data. *Cancer Discov.* **2**, 401–404 (2012).